Title
Parameterization of a calibrated geothermal energy pile model

Authors
Caulk, Robert
Ghazanfari, Ehsan
McCartney, John S

Publication Date
2016-03-01

DOI
10.1016/j.gete.2015.11.001

Peer reviewed

Parameterization of a calibrated geothermal energy pile model

Robert Caulk*, Ehsan Ghazanfari*, John S. McCartney**

Abstract

This paper describes the calibration and parameterization of a numerical model for conductive heat transfer from a group of geothermal energy piles into the soil surrounding the piles. Calibration was performed using Thermal Response Test (TRT) data collected from a group of full-scale in-situ geothermal energy piles in Colorado Springs, CO. The calibration of the three dimensional model incorporated field data to represent boundary conditions including inlet temperature, atmospheric temperature, and subsurface temperatures at different locations within the pile group. Following calibration, the model was parameterized to understand the role of heat exchanger configuration with a given energy pile as well as the role of pile spacing in an energy pile group. Parametric combinations were compared using heat transfer per unit length of the energy pile (W/m). The results of the parametric study indicate that heat transfer increases by up to 8% for an even heat exchanger layout compared to an uneven layout when considering a 15.2 m long, 0.61 m ⌀ energy pile configured with a W-shape heat exchanger. ~~energy~~

*Department of Civil and Environmental Engineering, University of Vermont, Burlington Vermont, USA

**Department of Structural Engineering, University of California San Diego, San Diego, California, USA

~~piles~~. These results also provide useful insight into the cross-sectional temperature distribution of the aforementioned energy pile configuration. ~~an energy pile.~~ Energy pile temperature was observed to vary by up to 20% across the core of the pile during heating for various heat exchanger layouts. This uneven temperature distribution may have implications on the estimation of in-situ thermal axial stresses in energy piles. Specifically, using measurements at strain gage locations may underestimate thermal axial stress during heating.

Keywords: Geothermal Energy, Energy Pile, Numerical Modeling, COMSOL, Calibration, Thermo-active foundation

1. Introduction

Indoor climate control accounts for almost 50% of America's residential energy consumption (EIA, 2011). As energy prices rise with increased demand and short supply, global communities will need clean renewable alternatives to heat/cool residential and commercial buildings. Although ground source heat pumps are a well-established energy efficiency technology, their coupling to building foundations provides a new way to transfer heat to or from the ground for lower installation costs. Heat is transferred by circulating heated or cooled fluid through closed-loop heat exchangers embedded in the foundations. In this way, geothermal energy piles serve two purposes, first to transfer building loads into the subsurface, but also to extract thermal energy from surrounding soils.

Concrete energy piles are a natural fit for geothermal energy. Since concrete foundation piles are generally longer than 6 m (Brandl, 2006), they provide access to the constant subsurface temperatures necessary for an efficient ground source heat pump (GSHP) system. Another benefit is the reduced heat exchanger installation cost compared to traditional vertical borehole heat exchangers. Since the installation of foundation piles requires drilling equipment, heat exchangers do not require additional installation (drilling) cost. Also, geothermal energy piles are easily coupled with solar panels to provide grid-independent climate control. Finally, the concrete protects the heat exchangers from damage and restrains potential ground water pollution (Brandl, 2006).

~~Geothermal energy piles need to remain operational for the lifespan of the building they are supporting. Therefore, t~~The initial geothermal energy pile design controls the heat transfer and ~~must maximize thermal performance and characterize the thermal~~ thermal stresses associated with the thermal soil-structure interaction for the lifespan of the foundation (Bourne-Webb et al., 2014). The cross-sectional temperature distributions within energy piles not only reflect the transient heat transfer characteristics of the geothermal energy pile, but may also have an important impact on the in-situ thermal axial stress within the energy pile (Murphy and McCartney, 2015). This study seeks to understand different aspects of geothermal energy pile behavior using a numerical model calibrated with field data. The specific objectives are to understand the role of heat exchanger configurations on heat transfer within the pile and on the thermal stress calculations. ~~The objective of this study is to employ numerical modeling~~

~~techniques to better understand the role of construction specifications on the thermal and thermo-mechanical performance of energy piles, as well as on their cross-sectional temperature distributions. Concrete cover, shank distance, and pile spacing contribute to both the amount of heat transferred from an energy pile into surrounding soils, as well as the cross-sectional temperature/thermal axial stress distribution. In the context of this study, concrete cover was defined as the minimum distance between the heat exchanger and the outer edge of the concrete pile and shank distance is defined as the width of the downward U loop heat exchangers as shown in Fig. 1.~~

In an attempt to provide insight into geothermal energy pile behavior, the present study details the calibration, validation, and parameterization of a model followed by a discussion of results and concluding remarks. COMSOL Multiphysics software and high-performance computing (HPC) enabled the construction of the full-scale three-dimensional finite element model. The model was calibrated with respect to an experimental field investigation conducted at the United States Air Force Academy (USAFA) in Colorado Springs, CO (Murphy et al., 2015). Accordingly, all geometries within the model reflect full-scale, in-situ geometries of the experimental energy piles and surrounding soil strata. The full-scale model coupled conductive heat transfer and non-isothermal pipe flow physics to estimate temperatures at any time/location within the model. Calibration was performed by comparing these model temperatures to field temperatures. Following calibration, the model was parameterized to understand the roles of concrete cover, shank distance (defined as the downwards U loop Fig. 1), and pile spacing on heat transfer from energy piles into surrounding soils. The heat transfer performance of the energy pile group was evaluated and relationships between construction specifications and performance were quantified. These relationships verified the model and enabled the investigation of the cross-sectional temperature distribution within the energy pile. These results were used to examine the implications of strain gage location on in-situ thermal axial stress estimation. In summary, this study exhibits the variation of energy pile performance with respect to construction specifications and the evolution of cross-sectional temperature distribution. ~~which is key to the improvement of geothermal energy piles.~~ Additionally, the study demonstrates the strength and flexibility of the finite element based model and the capabilities of COMSOL coupled with HPC.

2. Background

Evaluating heat transfer between geothermal energy piles and surrounding soils remains a key area of research numerically [Gao et al. (2008);Wood et al. (2009);Suryatriyastuti et al. (2012);Park et al. (2013);Abdelaziz et al. (2014); Gashti et al. (2014);Wang et al. (2014);Jalaluddin and Miyara (2014);Ozudogru et al. (2014)] and in the field [Laloui et al. (2006); Hamada et al. (2007); Bourne-Webb et al. (2009);Loveridge and Powrie (2012);Olgun et al. (2012);Murphy et al. (2015) ;McCartney et al. (2015); Abdelaziz et al. (2015)]. Field experiments performed by Hamada et al. (2007) and Gao et al. (2008) were designed to evaluate the most efficient heat exchanger layout within energy piles. With respect to thermo-mechanical processes, Bourne-Webb et al. (2009) used an experimental pile embedded in London Clay to investigate energy pile behavior during cyclic heating. More recently, Murphy et al. (2015) and Murphy and McCartney (2015) detailed the thermo-mechanical response of in-situ energy piles in different soil profiles. The interest in energy pile behavior has motivated the development of energy pile design guidelines.

A state of practice paper by Bourne-Webb et al. (2014) emphasized the current need for advanced finite element models in addition to field studies to improve existing design guidelines for geothermal energy piles. Existing energy pile design guidelines are contained within GSHPA (2012), however these guidelines focus on sizing and installation "best practices". In an attempt to move towards energy pile design guidelines that incorporate the thermally influenced pile-soil interface, Mimouni and Laloui (2014) conducted a combined numerical-experimental study. The study demonstrated the dynamic loading, expansion/contraction, and associated friction mobilization inherent to energy piles. Another key numerical study relating to the design of energy piles was performed by Cecinato and Loveridge (2015). The study investigated the influences of design parameters on energy pile efficiency using an analytically-validated numerical model and parametric statistical methods. These methods enabled the quantified contribution of several key design parameters including pile length, number of heat exchangers, and concrete cover. Cecinato and Loveridge (2015) expressed the importance of increasing the number of heat exchanger tubes to maximize efficiency. Different from the study of Cecinato and Loveridge (2015), this study incorporates full soil and foundation material calibration with the investigation of the role of design parameters on the cross-sectional temperature distribution for energy piles with W-shaped heat exchanger layouts.

Several other studies have focused on numerically and analytically modeling heat exchangers embedded within grout and concrete foundation piles. Abdelaziz et al. (2014) used a multilayer finite line source model of an energy pile to address ground stratification and thermally induced moisture migration. The study stressed the importance of incorporating multiple soil layers into any energy pile model. Ozudogru et al. (2014) validated a three dimensional COMSOL model with a finite line source analytical model and concluded that this methodology can successfully simulate the operation of heat exchangers embedded within soil. Gashti et al. (2014) investigated thermal regimes within steel energy piles using a three dimensional numerical analysis in COMSOL. The study yielded insight into the performance of U-tube configurations (1 vs 2 U-tubes) and a range of flow rates, however the main conclusion was that the thermal behavior within energy piles is inherently complex and requires three dimensional analysis (i.e. the assumption of a constant temperature along the length of an energy pile is insufficient to fully understand energy pile behavior). Another numerical study conducted by Kaltreider et al. (2015) investigated the design parameters of an energy foundation using a three dimensional numerical approach coupled with an experimental validation. The study focused on a U-shaped heat exchanger and concluded that flow rate, soil properties, and foundation depth contribute significantly to the heat flux from the floor slab to the building. Collectively, the aforementioned experiments and numerical/analytical investigations demonstrate the existing interest in heat exchanger layouts and the demand for a better understanding of the relationships between construction specifications and energy pile behavior/performance.

Many of the past and current energy pile field studies investigated the development of thermal axial strain and associated stresses within field piles using strain gages embedded within the piles (e.g. Murphy et al. (2015)). Murphy and McCartney (2015) observed that there may be issues in calculating the thermal axial stress in energy piles from strain gage measurements due to nonhomogenous cross-sectional temperatures within the energy piles. Specifically the strain within an energy pile is likely governed by the average cross-sectional temperature; however, the gage temperature may be up to 4^oC different than the average cross-sectional temperature (Loveridge and Powrie, 2013, Murphy and McCartney, 2015). Because the equation of the thermal axial stress requires knowledge of the change in average temperature of the pile (Murphy et al., 2015), this observation implies that using the temperature measured at a point to characterize the thermal axial stress may lead to errors in the stress calculation. This source of error was identified by Murphy and McCartney (2015), where the thermal axial strains during foundation heating were slightly greater than the free expansion thermal axial strains calculated using the temperature at a point. This means that the calculated thermal axial stress would be in tension, which does not make sense physically. Accordingly, a better understanding of temperature distribution may improve estimates of the changes in thermal axial stress in energy piles.

3. Governing equations

The use of the commercial COMSOL Multi-physics finite element software package enabled the three dimensional modeling of coupled interactions between heat exchangers embedded within concrete energy piles and stratified soils. Non-isothermal pipe flow and basic conductive heat transfer physics interacted within these three distinct domains (heat exchangers, concrete energy pile, soil). Several key parameters were accounted for to approximate the differential equations presented below (Ghasemi-Fare and Basu, 2013). Thermal conductivity, k, specific heat capacity, C_p, and density, ρ, of the soils, concrete piles, and embedded heat exchangers contributed to the rate and amount of heat transferred within the system. Heat transfer within the concrete energy pile and the surrounding soils was computed using the aforementioned material properties with the conservation of energy equation, assuming no internal heat generation:

$$\rho C_p \frac{\partial T}{\partial t} = \mathbf{\nabla} \cdot (k \mathbf{\nabla} T), \quad (1)$$

where ρ is density $[kg/m^3]$ and C_p is heat capacity at constant pressure $[J/(kg * K)]$. The right-hand side of the equation is the net rate of heat conduction into the material; k is the thermal conductivity $[W/(mK)]$ and T is the temperature of the material $[K]$.

Equivalent $(\rho C_p)_e$ and k_e values were used with Eq. 1 to compute heat transfer through porous media (Darcy porous medium):

$$(\rho C_p)_e = \theta_p \rho_p C_p + (1 - \theta_p)\rho_{soil} C_p, \tag{2}$$

$$k_e = \theta_p \rho_p + (1 - \theta_p) k_{soil}, \tag{3}$$

where $(\rho C_p)_e$ and k_e are the overall heat capacity and thermal conductivity per unit volume. The density and thermal conductivity of the pore fluid (in this case air) represented by ρ_p and k_p. Thus, $(1 - \theta_p)$ is the ratio of the area occupied by the solids to the total cross-sectional area of the soil.

In order to model the multi-physics problem presented by the energy piles, heat exchanger fluid flow must be incorporated (Gashti et al., 2014). The study presented here used one-dimensional pipe elements to represent the heat exchangers. This simplified pipe flow approximation was accomplished using the conservation of momentum and continuity equations (Barnard et al., 1966):

$$\rho \frac{\partial \boldsymbol{u}}{\partial t} = -\boldsymbol{\nabla_t} p \cdot \boldsymbol{e_t} - \frac{1}{2} f_d \frac{\rho}{d_h} |u| u, \tag{4}$$

$$\frac{\partial A\rho}{\partial t} + \boldsymbol{\nabla_t} \cdot (A\rho u \boldsymbol{e_t}) = 0, \tag{5}$$

where p is the pressure in the heat exchanger $[N/m^2]$, $\boldsymbol{e_t}$ is the tangential unit vector along the edge of the pipe, f_d is the darcy friction factor, ρ is the density of the fluid $[kg/m^3]$, d_h is the hydraulic diameter of the pipe $[m]$, and u is the velocity of the pipe flow $[m/s]$, and A is the cross-sectional area of the pipe $[m^2]$.

Heat transfer within the heat exchangers was computed using the conservation of energy for incompressible fluids within a pipe:

$$\rho A C_p u \boldsymbol{e_t} \cdot \boldsymbol{\nabla_t} T = \boldsymbol{\nabla_t} \cdot (Ak\boldsymbol{\nabla_t} T) + \frac{1}{2} f_d \frac{\rho}{d_h} |u| u^2 + Q_{wall}, \tag{6}$$

where T is the temperature of the entire pipe cross section $[K]$.

Finally, Q_{wall} within Eq. 6 accounts for the heat exchange through the HDPE tube with the concrete $[W/m]$:

$$Q_{wall} = h_{eff}(T_{ext} - T), \tag{7}$$

$$h_{eff} = \frac{2\pi}{\frac{1}{r_0 h_{int}} + \frac{1}{r_1 h_{ext}} + \frac{\ln(\frac{r_1}{r_0})}{k_{HDPE}}}, \tag{8}$$

where T_{ext} is the exterior temperature $[K]$, r_0 is the inner radius of the heat exchanger tube $[m]$, r_1 is the outer radius of the tube wall $[m]$, k_{HDPE} is the thermal conductivity of the HDPE heat exchanger tube, and h_{int} and h_{ext} are the film heat transfer coefficients determined by the Nusselt number of the flow (which depends on the Reynolds number, Prandtl number, and f_d).

Parametric combinations were compared by quantifying heat rejected (heat transferred) (W/m) (Eq. 9). This quantification of performance encourages a practical understanding of the parameter-operation relationship.

$$Q_{rejected} = c_w \rho_w q_{in} \frac{(T_{inlet} - T_{outlet})}{L_{pile}}, \tag{9}$$

where c_w is the specific heat capacity of the working fluid $[J/(kg * K)]$, ρ_w is the density of the working fluid $[kg/m^3]$, q_{in} is the flow rate $[m^3/s]$, and L_{pile} is the length of the energy pile $[m]$.

4. Summary of test site

The calibration of the model was performed using temperature data collected by (Murphy et al., 2015) from a group of eight energy piles installed beneath an unfinished and atmosphere-exposed 1-story building on the USAFA campus in Colorado Springs, CO (Fig. 2). Specifically, the spatial and temporal variations in foundation and subsurface temperatures were used to calibrate the conductive heat transfer model implemented in COMSOL and presented in this paper. Four of the eight installed foundation piles were modeled during this study. Together, the four cylindrical energy piles were connected in parallel to the heat pump and were equipped with replicate configurations - diameters of 0.61 m (meters), lengths of 15.2 m, and W-shaped heat exchangers (Fig. 3b). The inlet and outlet heat exchange ports were placed 90^o apart and the heat exchangers were attached to the inside of the rebar cage - approximately 0.46 m in diameter. These heat exchangers were 19 mm diameter HDPE tubes with 3 mm wall thicknesses. As-built energy piles included strain gauges attached to the inside of the rebar cage (Fig. 4a) ~~embedded instrumentation~~ to infer the change in temperature and thermal axial strain at several depths. Further, the soil surrounding the energy piles included an array of thermistors at different depths and radial locations. These thermistors had a precision of 0.1^oC and were used to infer the heat transfer away from the energy piles. Another important site characteristic was the level of saturation of the subsurface. The water table was not observed during the installation of the piles and prior field investigations indicated that the water table was at least 70 m below the surface. Additionally, during the period of the heating test there were no significant rainstorms, so the soil conditions were considered unsaturated for this study. A layout of the energy pile group supporting the 1-story building, as well as the surrounding array of observational equipment is shown in Fig. 2b.

Foundations 1-4 were evaluated during a Thermal Response Test (TRT) carried out during the summer of 2013. During the two-stage TRT, the heat pump supplied constant power to the circulating fluid for 500 hours after which the flow was stopped while sensors monitored the ground response for an additional 1,200 hours. In an attempt to observe the reaction of the piles and surrounding soils, the network of strain and temperature monitors collected data at five-minute intervals for the total duration 1,700 hours. Murphy et al. (2015) used these observations experimentally to characterize thermo-mechanical response within the energy piles. The current study used the field-collected data to construct, calibrate, and validate a numerical model. Following calibration/validation, the model was used to gain insight into energy pile behavior with respect to construction specifications (concrete cover, shank distance, pile spacing).

5. Model details

COMSOL model geometry (Fig. 3a) matches the experimental group of piles shown in Fig. 2 and described in Sec. 4. The soil block surrounding the piles measured 40 m x 21 m x 22.5 mm and ensured 15 m between the pile and any subsurface boundary conditions, thus avoiding unnecessary boundary condition interaction.

The model geometry was constructed within COMSOL software. COMSOL encourages parameterization by allowing the user to build geometry based on variables (e.g. concrete cover, shank distance, pile diameter, pile length, etc.). In this way, multiple simulations can be run for a specific variable.

6. Material Properties

Material properties were assigned to their respective domains to simulate reality as closely as possible. Properties of the stratified soil block, concrete piles, HDPE heat exchanger tubes, glycol-water working fluid, and atmospheric air are detailed in Table 1. Material densities reported by Murphy et al. (2015) were assigned to respective materials within the model, while remaining properties required for the heat transfer model were adjusted during calibration, as detailed in Section 9. These properties included thermal conductivity, specific heat capacity, and porosity.

7. Boundary conditions

All boundary conditions were imposed on the model using data collected from the field experiment detailed by Murphy et al. (2015). These observation based boundary conditions were applied as variable interpolation functions.

Atmospheric temperature observations (Fig. 5) were applied to the top surface of the model (Fig. 3a) with a transient Dirichlet temperature boundary condition. In an attempt to mimic reality, a thin layer of insulating air (50 mm) was used as a buffer between the temperature boundary condition and the soil/concrete slab. This buffer was modeled as purely conductive heat transfer associated with the lower density, lower thermal conductivity, and higher heat capacity of air compared to the subsurface (Table 1). ~~This more accurately reflected reality and avoided error resulting from direct application of atmospheric temperature to soil~~

~~surface .~~

Subsurface temperature gradient measurements were applied as the initial condition and boundary conditions ~~to the boundaries~~ of the soil block with a variable (with depth) Dirichlet temperature boundary condition. Two additional Dirichlet boundary conditions were applied to the inlet of the heat exchanger tubes: transient flow and temperature. The flow conditions within the heat exchangers were variable with time to simulate the two-stage TRT. First the flow was 106 ml/s for the 500 hours, followed by 1,200 hours of 0 ml/s. Inlet temperatures collected from the field (Fig. 6) were directly applied to the boundary condition within the model. Additionally, the inlet temperatures for each of the four foundations varied by less than 0.5 ^{o}C. This consistency allowed the study to incorporate a symmetric boundary condition.

Finally, an adiabatic symmetric boundary condition was used to model only two of the four piles active during the TRT (Fig. 3b). The adiabatic boundary condition decreased the computational cost and resulted in a higher density mesh.

8. Convergence study

Careful attention was paid to building the equilateral triangular finite-element mesh for the numerical USAFA energy pile model. The distribution of elements was optimized using a convergence study that ensured a sufficient level of accuracy while minimizing computational time and resources. The global domain encompassing the 19,000 m^3 stratified soil block, two 15.2 m long x 0.61 m diameter concrete energy piles, a 50 mm thick concrete slab, and a 50 mm-thick layer of air was partitioned into four respective subdomains. A convergence study was first performed on the concrete pile subdomain. Maximum pile temperature was selected as the characteristic output parameter. ~~It was clear that these piles required a high density of elements to closely approximate temperature distribution.~~ Minimum element size, growth rate, and resolution were manipulated until the output parameter reached $\Delta T_{max} < 0.1^oC$ (corresponding to a 0.33% change in ^oC) between mesh refinement steps. Final pile domain element size was ≈0.04-0.07 m depending on the heat exchanger geometry. Following the conclusion of the concrete pile mesh refinement, the soil block mesh was studied. Again, maximum soil block temperature was used as the characteristic output parameter. Element growth rate and minimum element size were manipulated until the output parameter reached $\Delta T_{max} < 0.1^oC$. Final soil block domain element sizes ranged from 0.07 m near the piles to 0.8 m near the boundaries of the model. Lastly, the air and concrete slab domains were not considered during the mesh refinement study, because the purpose of these domains was strictly for insulation. Therefore, these meshes were reduced to the minimum number of elements necessary to achieve the observed insulating characteristics during the calibration phase. The associated element sizes for these domains correspond to the largest equilateral triangle allowed within the domain - 0.058 m. The final average equilateral element quality (measure for how equilateral the elements are, 0-1.0) for the global domain was 0.81 for $\approx 600,000$ elements, which ensured that the elements were distributed in a way that captured the heat transfer in the most efficient manner possible without sacrificing solution accuracy. The refined mesh is shown in Fig. 7.

9. Calibration and validation

The calibration process attempted to match model output to field observations by adjusting thermal conductivities, heat capacities, and soil porosities. The field investigation did not thoroughly characterize thermal conductivity and heat capacity versus depth; thermal conductivity and heat capacity values were obtained from point measurements on split-spoon soil samples extracted during site investigation using a dual-needle thermal probe. These specimens were likely slightly disturbed due to the mode of sampling (standard penetration testing), so they may not represent the actual thermal properties in-situ. Accordingly, these thermal properties were used as a baseline guess during the calibration process, then were varied in a controlled manner with depth to match the observed heat exchanger fluid and ground temperatures in the thermal response test. This calibration approach was used to both capture trends in the observed data, but also to refine the properties of the soil stratigraphy to match the observed changes in ground temperature with depth during the thermal response test. The porosities of the soil in the field were not measured, but typical values for a dense sandstone were selected for use in the models.

The preliminary calibration of the model was detailed in Caulk et al. (2014) and the final calibration presented here yields a model with improved accuracy. The improved accuracy was due primarily to the improved mesh (described in Section 8) and further discretization of soil porosities. The method used for calibration was straightforward. First, the soil heat transfer properties were set to field collected values. Heat exchanger outlet fluid temperatures were then compared to field outlet temperatures. Since these values matched well (Fig. 6), nearby in-situ borehole and foundation temperatures were used to adjust soil heat transfer properties. These field data were stamped with time and location (x,y,z) and were collected at five minute intervals for a duration of 1,700 hours (71 days) (exact locations are shown in Fig. 2). First, for 500 hrs of active energy pile heat rejection q=106 ml/s, followed by 1,200 hrs of cooling observation q=0 ml/s. Calibration was performed by comparing model output to in-situ temperatures during active heat rejection (time=214 and 500 hours) and adjusting soil heat transfer properties accordingly. Finally, validation was performed by comparing model output to in-situ temperatures following cooling (time=1,700 hours).

Field data along the length of Foundation 4, Borehole 4 (BH4), and Borehole 6 (BH6) were compared to temperature data output by the COMSOL model as shown in Fig. 8. BH4 & BH6 were selected due to diversity of distance from Foundation 4 and coverage/no coverage by concrete slab. ~~exposure/non-exposure to atmospheric conditions.~~ BH4 represents several depths of observation beneath the concrete slab close to Foundation 4 (1.22m), while BH6 represents several depths of observation exposed to atmospheric conditions and further from Foundation 4 (2.44m). Initial observations of field data and model output align with expectations - the less distant and covered BH4 is more greatly affected by the active energy piles within the highly conductive sandstone layer (2-12 m), while the distant and uncovered BH6 was more greatly affected by the atmospheric temperature within the shallow sandy fill (1-2 m)(Fig. 8).

The comparison of field data to model output at the aforementioned locations dictated the calibration of thermal conductivities, heat capacities, and porosities of individual soil layers. Although there are many combinations of the aforementioned parameters that might result in the same amount of heat transferred (Wagner et al., 2012), this study minimized the number of possible combinations by limiting the available thermal conductivity parameter options to a small range around those reported by Murphy et al. (2015). Heat capacity and porosity ~~These~~ values were adjusted more significantly to minimize the differences between the model temperature output and the field temperature observations. Even so, the final calibrated heat capacity and porosity values match those associated with the respective materials. Finally, soil and rock densities were not altered from those reported by Murphy et al. (2015). Once the heat transfer properties were set, model output was compared to field measurements for validation purposes. Final calibrated properties agree with values published in Murphy et al. (2015) (see Table 1) and generally accepted heat capacity (Eppelbaum et al., 2014) and porosity values for sandy soil and sandstone rock.

The final calibrated and validated model results are shown in Fig. 8 and Fig. 9. The calibrated model matched the field collected data well; the RMSE for Foundation 4, BH4, and BH6 were 0.97, 0.67, and 0.82 ^{o}C, respectively. Model output error was calculated between the model predicted and measured temperatures as follows (see Tables 2, 3, and 4):

$$error = abs(((measured - predicted)/measured))X100\% \tag{10}$$

Greater error was observed at the shallow depths of 0.6-1.8 m and the long duration of 1700 hours. These higher errors at shallow depths may be a result of surface phenomena that was not accounted for within this model (e.g. rain, wind, solar radiation). In comparison, BH4 remained protected by a concrete slab throughout the duration of the experiment and exhibited higher accuracy temperature predictions after 500 hrs at the surface compared to BH6, which was exposed to the atmosphere for the duration of the TRT. Error associated with the validated long duration of 1,700 hours can be attributed to model propagated error.

10. Results and discussion

10.1. Effects of concrete cover and shank distance

Concrete cover and shank distance are both construction specifications that affect the performance of an energy pile (Caulk and Ghazanfari, 2015). Concrete cover is defined as the minimum distance between the heat exchanger tube and the outer edge of the concrete pile (Fig. 1). This construction/design specification is generally controlled by the necessity to protect reinforcing steel, provide thermal insulation, and maintain stresses. Energy pile design should consider concrete cover as an important piece of the design since heat exchangers are fixed to the ~~inside of the~~ reinforcing steel cage.

Similar to concrete cover, shank distance is a construction specification that is easily modified. Shank distance describes the width of the downwards U of a heat exchanger as shown in Figures 1 and 4. These simple specifications can impact the performance of an energy pile. Therefore, this study used a calibrated numerical model of a group of energy piles to investigate the impact of concrete cover and shank distance on energy pile performance.

It would be expected that these specifications are optimized upon even distribution throughout the pile (i.e. the tubes are equidistant from their direct neighbors)(Fig. 4). Even heat exchanger distribution yields an evenly heated pile cross-section which leads to the maximum energy pile performance (Eq. 9). This study attempted to verify this assumption numerically, and quantify the performance increase/decrease with respect to concrete cover and shank distance.

The model was simulated for 500 hours and was constrained by the same inlet fluid temperatures and subsurface temperature gradients as the TRT. ~~boundary~~

~~conditions as described in Sec. 7 and Sec. 9~~. Simulations were performed for a range of concrete covers (0.04-0.145 m) and shank distances (0.10-0.45 m). The final $\Delta T(500hrs)$ was used with Eq. 9 to determine the quantity of heat rejected for each parameter combination as shown in Fig. 10.

Concrete cover plays an important role in total heat rejected. For a shank distance of 0.35 m, an increase of concrete cover from 0.04 to 0.11 m yielded a 9.7 % decrease in heat rejected. These results confirm findings in the literature (Cecinato and Loveridge, 2015, Caulk and Ghazanfari, 2015); as concrete cover is increased, heat rejected is decreased. Shank distance also contributes to final energy pile performance. For a concrete cover of 0.04 m, shank distance increased pile heat rejected by 8.3 % (0.1-0.325 m shank distance, where 0.325 m corresponds to an even heat exchanger layout). However, beyond the shank distance associated with even heat exchanger layout, the amount of heat rejected decreased due to the redevelopment of an uneven heat exchanger layout.

These results verify the model by proving its sensitivity to small changes in cross-sectional heat exchanger configuration. Evenly spaced heat exchangers yielded the best energy pile performance due to an evenly heated cross-section (Fig. 10), while even small changes to heat exchanger layout reduced the energy pile performance due to an unevenly heated cross-section. This model verification enabled the investigation of cross-sectional temperature distribution and its role in the approximation of thermal axial stresses.

10.2. Cross-sectional temperature distribution

The cross-sectional temperature distribution of an energy pile plays a key role in thermal axial stress estimation via strain/temperature gages. The approximation of in-situ thermal axial stress relies on the temperature and strain at the location of the gage as follows:

$$\sigma_T = E(\epsilon_T - \alpha_c \Delta T), \tag{11}$$

where σ_T is the thermal stress [MPa] as a function of Young's modulus (E) [MPa], thermal strain (ϵ_T), coefficient of linear expansion of concrete (α_c) [$\mu\epsilon/^oC$], and temperature (ΔT) [^oC]. Positive σ_T and ϵ_T values indicate compression as a result of heating expansion, which means α_c must be defined as a negative value to accommodate for positive ΔT values during heating.

Thermal strains (ϵ_T) reported by Murphy et al. (2015) were computed using the difference between the fluctuating thermal strain caused by the restrained thermal expansion or contraction of the concrete (ϵ_i) and the initial strain due to the building load (ϵ_0). Thermal axial stresses were then calculated using Eq. 11, which relies on ϵ_T and ΔT at the point of the gage. Murphy et al. (2015) extended the study by plotting the thermal axial strain as a function of ΔT and depth. The slopes of these data were considered the ~~evaluating the thermal axial strain as a function of~~ ~~ΔT~~ ~~at several depths, which enabled the estimation of~~

~~a~~ mobilized coefficients of thermal expansion, α_{mob} [$\mu\epsilon/^oC$] ~~with depth~~. Since α_{mob} is a function of ΔT and depth, the study presented in this paper estimated theoretical thermal axial stresses using the following equation:

$$\sigma_{T,theo} = E((\alpha_{conc,free} - \alpha_{mob})\Delta T) \tag{12}$$

where $\sigma_{T,theo}$ is the theoretically determined thermal axial stress [MPa] and α_{free} is the coefficient of free expansion for reinforced concrete [$\mu\epsilon/^oC$], -12 $\mu\epsilon/^oC$.

Since the cross-sectional temperature distribution can vary by up to 4^oC (Loveridge and Powrie, 2013), ϵ_T and ΔT at the location of the gage may contribute to an under/overestimated thermal stress. Therefore, this study used a calibrated model of a group of energy piles to demonstrate the evolution of cross-sectional temperature and stress distribution. For this analysis, the model was simulated for 500 hours and was constrained by the same inlet fluid temperatures and subsurface temperature gradients as the TRT. ~~boundary conditions as described in Sec. 7 and Sec. 9.~~ The model was probed for ~~Probes were used to extract~~ cross-sectional temperatures ~~within the model~~ (Fig. 4). Time and location stamped temperatures were then post-processed to compute theoretical cross-sectional thermal stresses (Eq. 12).

Fig. 11 shows the evolution of cross-sectional temperature/thermal axial stress distribution with time for an even heat exchanger layout (Fig. 4a) at 7.6m depth. At 10 hours, the distribution was relatively even, but by 250 hours the core of the pile stabilized to 4^oC above the strain gage. The corresponding thermal axial stress difference between the core and the strain gage stabilized to 0.88 MPa after 250 hours. This difference corresponds to a thermal axial stress increase of 20% between the strain gage and the core for the duration of the TRT.

The temperature distribution with respect to the primary and secondary cross-sections (Fig. 4a) varied depending on the shank distance and concrete cover. As expected, the evenly distributed heat exchangers (Fig. 4a) yielded the most evenly distributed temperature/thermal axial stress; cross-sectional temperatures and stresses varied by $\approx 0.3^oC$ and 0.06 MPa (Fig. 11) around the perimeter, respectively. Conversely, the extreme shank distances of 0.1 m and 0.45 m (Fig. 4b&c) yielded the least evenly distributed temperature/thermal stress; cross-sectional temperatures and stresses varied by $\approx 8^oC$ and 1.71 MPa around the perimeter (Fig. 12a and 12b). Furthermore, these extreme combinations also exhibited thermal axial stress differences of $\approx$ 1.15 MPa between the strain gage and the core.

These results also shed light on energy pile performance. The energy pile performance corresponding to the parameter combinations used to build Figures 11, 12a, and 12b are shown in Fig. 10. The uneven temperature distributions of Fig. 12a & 12b correspond to a decrease of heat rejected by $\approx$ 8%. Conclusively, the evenly spaced heat exchanger layout corresponds to higher energy pile performance.

10.3. Effect of pile spacing

Pile spacing may be dictated by structural design, geotechnical investigations, or foundation design. Therefore, this design specification may not be as simple to manipulate as concrete cover or shank distance. However, this study used the calibrated/validated model to quantify the relationship between pile spacing and energy pile performance. Results from this exercise were used to support findings in the literature and further verify the model.

The model was simulated for 500 hours and was constrained by the same boundary conditions as described in Sec. 7 and Sec. 9. Simulations were performed for a range of pile spacings (0.5-16 m). For each value of pile spacing, the soil block was adjusted to maintain the same distance between the pile and the boundary conditions. This boundary adjustment isolated the pile spacing as the only parameter that contributed to changes of heat rejected. The final $\Delta T(500hrs)$ was used with Eq. 9 to determine the performance of each pile spacing.

Fig. 13 exhibits the performance of the energy piles with respect to pile spacing. As expected, the heat rejected increases with increased pile spacing. An increase of 4 m (1-5 m) increased heat rejected by 21.7%. As the pile spacing increases, the thermal gradient between the pile and surrounding soils remains greater for a longer period of time, resulting in more heat rejected. Conversely, the thermal gradient decreases as the piles approach one another. This decreased thermal gradient is due to the heated soil nearby the neighboring pile resulting in a lower thermal gradient, lower heat rejected, and lower pile performance.

These results further verify the model and support findings from the literature. Morino and Oka (1994) used a validated numerical model to investigate the temperature distribution surrounding a 20 m long, 40 cm ⌀ steel pile after 480 hours of active heat adsorption. The study concluded that the soil temperature remained undisturbed 3 m from the energy pile. Although pile geometry, fluid temperatures, and initial conditions could affect any study comparison, Fig. 13 shows that performance plateaus for two piles spaced $\approx$6 m, which supports the results within Morino and Oka (1994).

11. Conclusions

The calibration, validation, and parameterization of a full-scale geothermal energy pile model was performed using advanced finite element analysis software and HPC. Final results from the parametric study verified the model and provided insight into the relationship between model parameters and energy pile performance. The validated model was also used to analyze the evolution of the cross-sectional temperature/thermal stress.

Full calibration of the three-dimensional model required detailed boundary conditions, discretized soil layers, and extensive field data. All boundary conditions were variable with time or space, and were imported directly from the field data (atmospheric temperatures, subsurface temperature gradients, inlet temperatures, etc.) Several layers of soil were used to calibrate the model output to the field data. Each soil layer was identified by several unique material properties, namely, heat capacity, thermal conductivity, and porosity. These properties were carefully calibrated using time series temperature data at nine depths within the concrete energy pile and six depths within the surrounding soils.

The amount of heat rejected from an energy pile into surrounding soils with respect to geometrical parameters was quantified by model parameterization. Energy pile performance was evaluated as a function of concrete cover, shank distance, and pile spacing. This parametric sweep verified the original assumption that the optimal heat exchanger configuration (combination of concrete cover and shank distance) is the configuration that maintains equal distances between heat exchanger pipes (in cross-section view). Additionally, this parametric sweep quantified the loss of performance as pipes become less evenly distributed. A change of heat exchanger configuration can alter performance by up to 8% when considering a 15.2 m long, 0.61 m ⌀energy pile configured with a W-shape heat exchanger. Furthermore, the parametric sweep verified the sensitivity of the model to cross-sectional temperature distributions.

Upon validation of the model, the evolution of the cross-sectional temperature/thermal axial stress distribution during a heating cycle was investigated. The result of this investigation demonstrated the under/over estimation of thermal axial stress reported by field experiments. In particular, the USAFA experiment used to calibrate the model was reliant on embedded strain gages to compute thermal stress. These strain gages were attached to the reinforcing cage at the perimeter of each pile. This study showed that the thermal stress computed at the perimeter of the pile versus the core may vary by up to 1.71 MPa. Furthermore, the heat exchanger layout has a significant impact on temperature/stress distribution. For certain combinations of concrete cover and shank distance, the stress varied by up to 1.15 MPa at different locations around the perimeter of the pile. These results draw several conclusions about the approximation of temperature/thermal axial stress distribution within piles:

1. Cross-sectional thermal axial stress within energy piles is not constant. During heating, the thermal axial stress may be as much as 20% greater at the core of the pile than the reinforcing cage. This should be considered for stress analyses on in-situ energy piles.
2. Evenly distributed heat exchangers distribute temperature and thermal axial stress evenly around the perimeter of the pile, while uneven heat exchanger layouts exhibit extreme temperature/thermal axial stress variance across the core and around the perimeter of the pile.
3. The performance of an energy pile depends strongly on its cross sectional temperature distribution. This study demonstrated that even heat exchanger layouts correspond to even cross-sectional temperature distributions, which correspond to higher energy pile performance.

The research presented here demonstrates the need for energy pile stress and performance design standards. Results indicate that priority should be set on an even heat exchanger layout and lower concrete cover to mitigate axial stress mobilization and increased heat transfer, respectively. Further, in-situ temperature and strain measurements may vary by up to 20% depending on where within the pile cross section they are measured. Future in-situ energy pile experiments should be aware of this variation, while historical in-situ stress studies should be cited with this variation in mind.

12. Acknowledgements

The authors acknowledge the Vermont Advanced Computing Core, which is supported by NASA (NNX 06AC88G), at the University of Vermont for providing High Performance Computing resources that have contributed to the research results reported within this paper.

References

Abdelaziz, S. L., Olgun, C. G., and Martin, J. R. (2015). Equivalent energy wave for long-term analysis of ground coupled heat exchangers. *Geothermics*, 53:67–84.

Abdelaziz, S. L., Ozudogru, T. Y., Olgun, C. G., and Martin, J. R. (2014). Multilayer finite line source model for vertical heat exchangers. *Geothermics*, 51:406–416.

Barnard, A. C., Hunt, W. A., Timlake, W. P., and Varley, E. (1966). A theory of fluid flow in compliant tubes. *Biophysical Journal*, 6:717–724.

Bourne-Webb, P., Pereira, J., Bowers, G., Mimouni, T., Loveridge, F., Burlon, S., Olgun, C. G., McCartney, J. S., and Sutman, M. (2014). Design tools for thermoactive geotechnical systems. *DFI Journal: The Journal of the Deep Foundations Institute*, 8(2):121–129.

Bourne-Webb, P. J., Amatya, B., Soga, K., Amis, T., Davidson, C., and Payne, P. (2009). Energy pile test at Lambeth College, London: geotechnical and thermodynamic aspects of pile response to heat cycles. *Geotechnique*, 59(3):237–248.

Brandl, H. (2006). Energy foundations and other thermo-active ground structures. *Géotechnique*, 56(2):81–122.

Caulk, R. and Ghazanfari, E. (2015). Investigation of construction specification effects on energy pile efficiency. In *Proceedings of the International Foundations Conference and Equipment Exposition (IFCEE 2015)*, pages 1648–1657, San Antonio, TX. Mar. 17-21. ASCE.

Caulk, R., McCartney, J., and Ghazanfari, E. (2014). Calibration of a geothermal energy pile model. In *Proceedings of the COMSOL Boston 2014 Conference*, Boston, MA. COMSOL.

Cecinato, F. and Loveridge, F. (2015). Influences on the thermal efficiency of energy piles. *Energy*, 82:1021–1033.

EIA (2011). Annual Energy Review. Technical report, Energy Information Administration.

Eppelbaum, L., Kutasov, I., and Pilchin, A. (2014). Thermal Properties of Rocks and Density of Fluids. In *Applied Geothermics*, Lecture Notes in Earth System Sciences, pages 99–142. Springer-Verlag Berlin Heidelberg, Berlin, Heidelberg.

Gao, J., Zhang, X., Liu, J., Li, K., and Yang, J. (2008). Numerical and experimental assessment of thermal performance of vertical energy piles: An application. *Applied Energy*, 85(10):901–910.

Gashti, E. H. N., Uotinen, V. M., and Kujala, K. (2014). Numerical modelling of thermal regimes in steel energy pile foundations: A case study. *Energy and Buildings*, 69:165–174.

Ghasemi-Fare, O. and Basu, P. (2013). A practical heat transfer model for geothermal piles. *Energy and Buildings*, 66:470–479.

GSHPA (2012). Thermal Pile Design , Installation and Materials Standards. Technical Report October 2012, Ground Source Heat Pump Association.

Hamada, Y., Saitoh, H., Nakamura, M., Kubota, H., and Ochifuji, K. (2007). Field performance of an energy pile system for space heating. *Energy and Buildings*, 39(5):517–524.

Jalaluddin and Miyara, A. (2014). Performance investigation of multiple-tube ground heat exchangers for ground-source heat pump. *American Journal of Energy Engineering*, 2(5):103–107.

Kaltreider, C., Krarti, M., and McCartney, J. S. (2015). Heat transfer analysis of thermo-active foundations. *Energy and Buildings*, 86:492–501.

Laloui, L., Nuth, M., and Vulliet, L. (2006). Experimental and numerical investigations of the behaviour of a heat exchanger pile. *International Journal for Numerical and Analytical Methods in Geomechanics*, 30:763–781.

Loveridge, F. and Powrie, W. (2012). Performance of piled foundations used as heat exchangers. In *18th International Conference for Soil Mechanics and Geotechnical Engineering*, pages 3371–3374. ICE Geotech Eng.

Loveridge, F. and Powrie, W. (2013). Temperature response functions (G-functions) for single pile heat exchangers. *Energy*, 57:554–564.

McCartney, J. S., Murphy, K. D., and Henry, K. S. (2015). Response of an energy foundation to temperature fluctuations. In *Proceedings of the International Foundations Conference and Equipment Exposition (IFCEE 2015)*, pages 1691–1700, San Antonio, TX. Mar. 17-21. ASCE.

Mimouni, T. and Laloui, L. (2014). Towards a secure basis for the design of geothermal piles. *Acta Geotechnica*, 9(3):355–366.

Morino, K. and Oka, T. (1994). Study on heat exchanged in soil by circulating water in a steel pile. *Energy and Buildings*, 21(1):65–78.

Murphy, K. D. and McCartney, J. S. (2015). Seasonal response of energy foundations during building operation. *Geotechnical and Geological Engineering*, 33(2):343–356.

Murphy, K. D., McCartney, J. S., and Henry, K. S. (2015). Evaluation of thermo-mechanical and thermal behavior of full-scale energy foundations. *Acta Geotechnica*, 10(2):179–195.

Olgun, C. G., Martin, J., Abdelaziz, S., Iovino, P. L., Catalbas, F., Elks, C., Fox, C., and Gouvin, P. (2012). Field testing of energy piles at Virginia Tech. In *Proceedings from the 37th Annual Conference on Deep Foundations*, Houston, TX.

Ozudogru, T., Olgun, C., and Senol, A. (2014). 3D numerical modeling of vertical geothermal heat exchangers. *Geothermics*, 51:312–324.

Park, H., Lee, S., Yoon, S., and Choi, J. (2013). Evaluation of thermal response and performance of PHC energy pile: Field experiments and numerical simulation. *Applied Energy*, 103:12–24.

Suryatriyastuti, M. E., Mroueh, H., and Burlon, S. (2012). Understanding the temperature-induced mechanical behaviour of energy pile foundations. *Renewable and Sustainable Energy Reviews*, 16:3344–3354.

Wagner, V., Bayer, P., Kübert, M., and Blum, P. (2012). Numerical sensitivity study of thermal response tests. *Renewable Energy*, 41:245–253.

Wang, W., Regueiro, R. A., and McCartney, J. S. (2014). Coupled axissymmetric thermo-poro-elasto-plastic finite element analysis of energy foundation centrifuge experiments in partially saturated silt. *Geotechnical and Geological Engineering*, 33(2):373–388.

Wood, C. J., Liu, H., and Riffat, S. B. (2009). Use of energy piles in a residential building , and effects on ground temperature and heat pump efficiency. *Geotechnique*, 59(3):287–290.

List of Figures

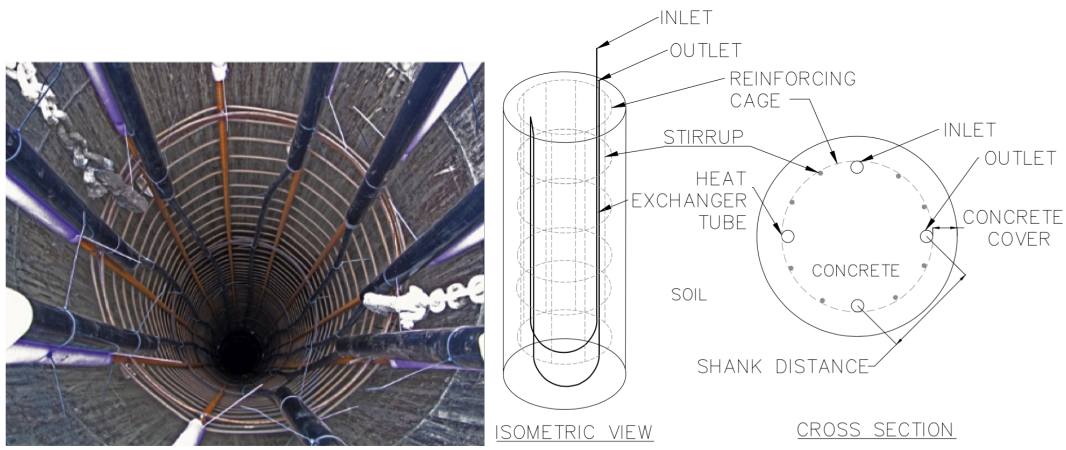

Figure 1: Image and sketch showing heat exchanger pipes embedded in concrete energy piles with geometry details relevant to thermal performance

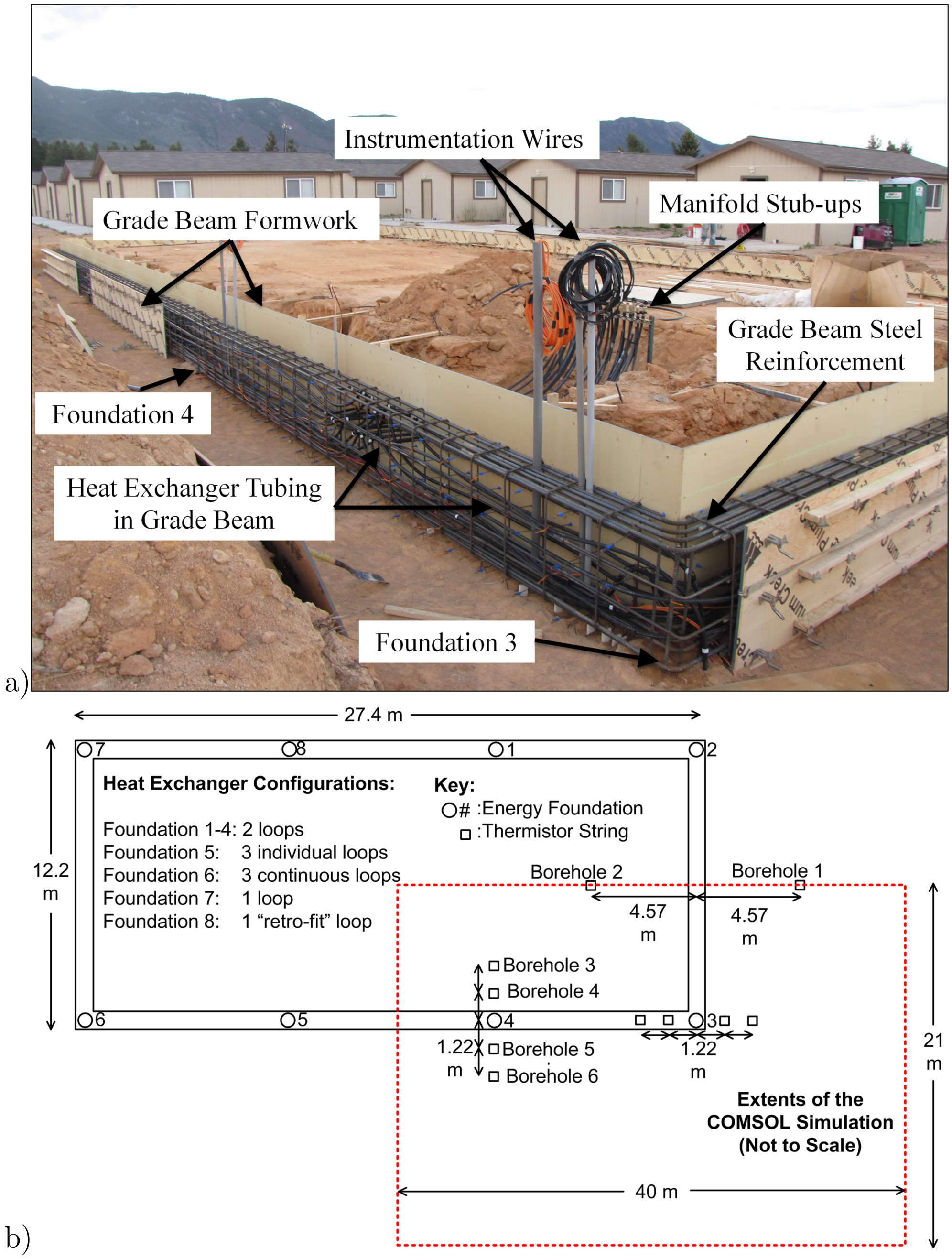

Figure 2: USAFA experimental pile group a) construction picture b) plan view (Murphy et al., 2015)

a)

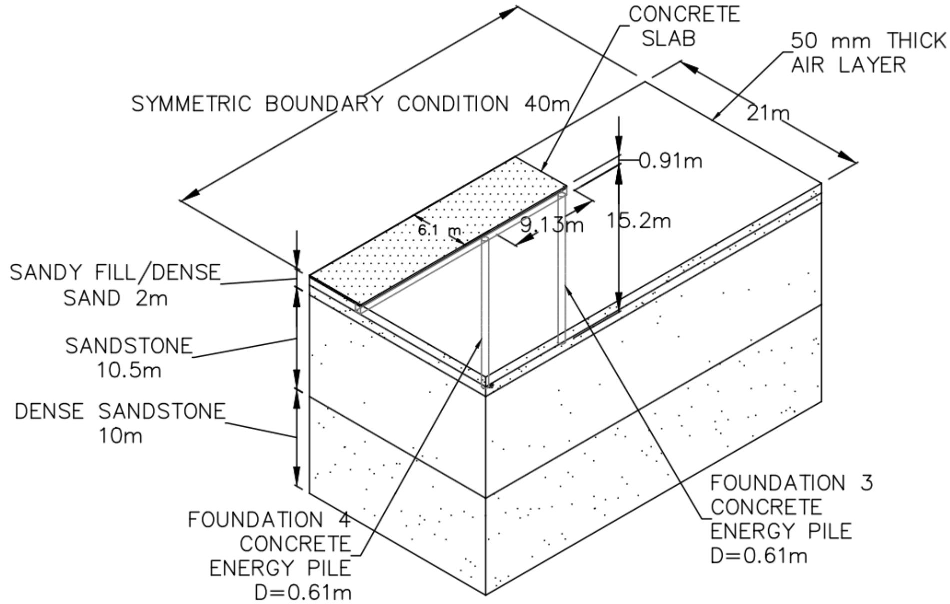

b)

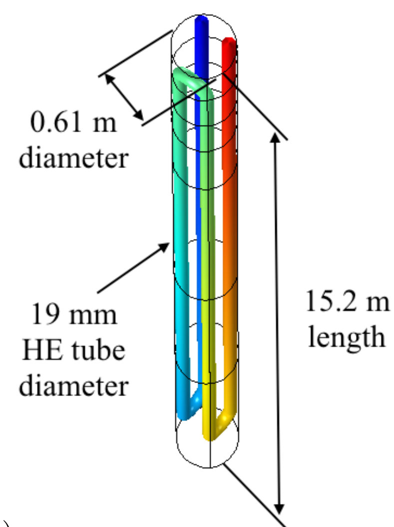

Figure 3: COMSOL model geometry a) Full model b) close up of Foundation 4

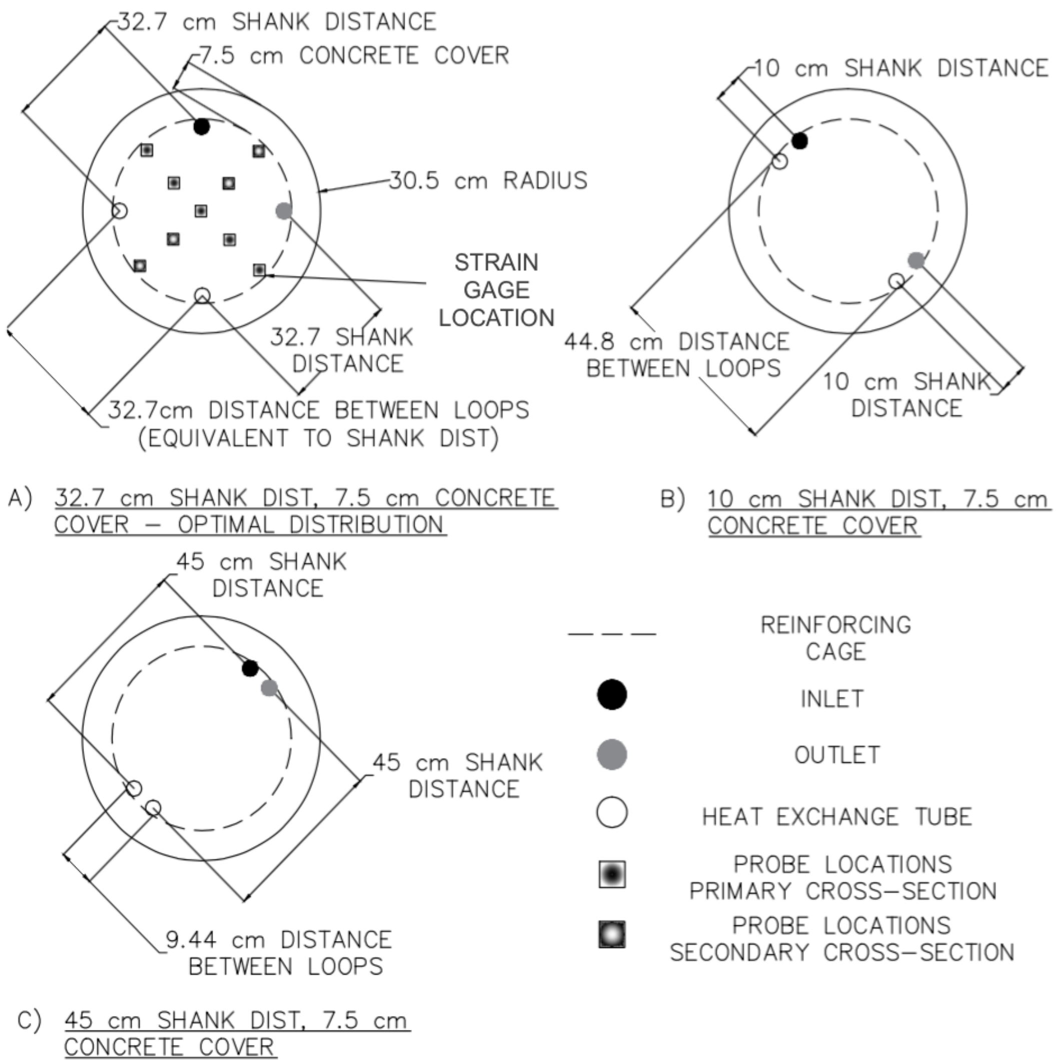

Figure 4: Shank distance parameterization and probe locations

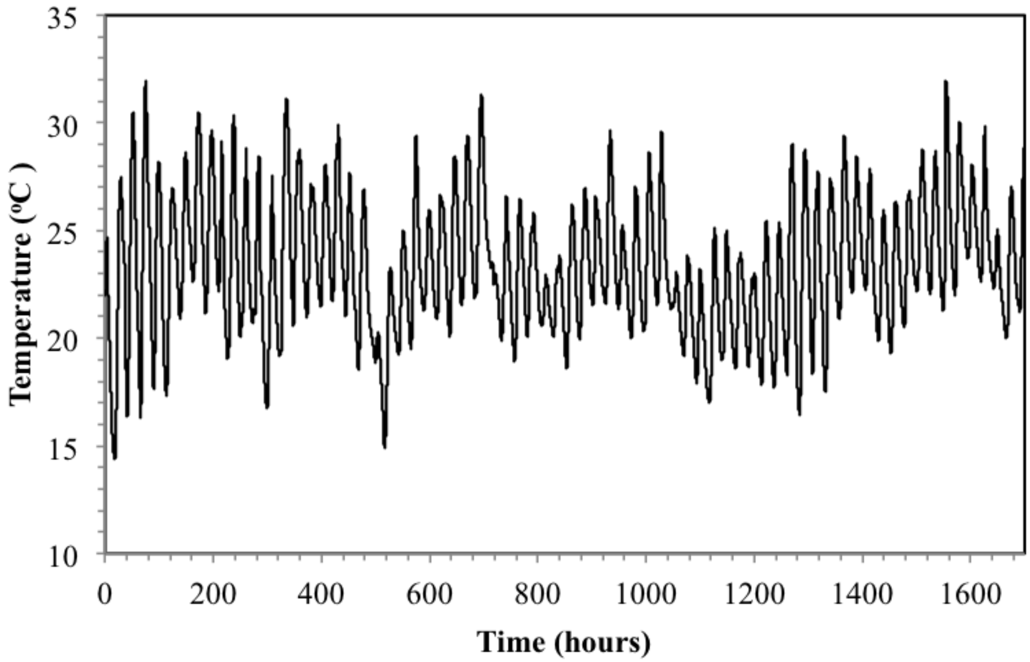

Figure 5: Known atmospheric temperature boundary condition applied to the model during the duration of the thermal response test

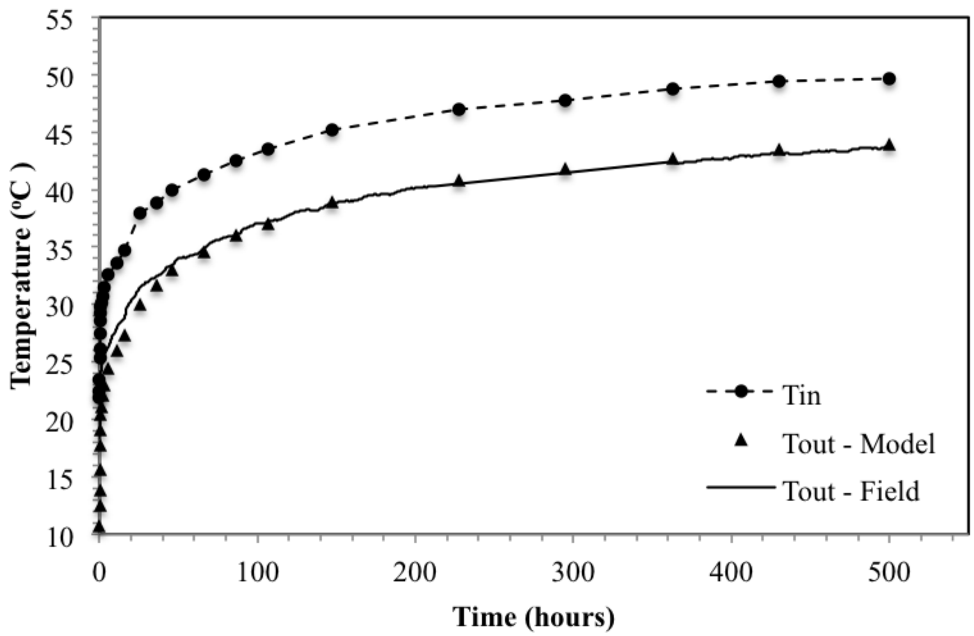

Figure 6: Heat exchanger inlet temperature applied as the boundary condition to the model

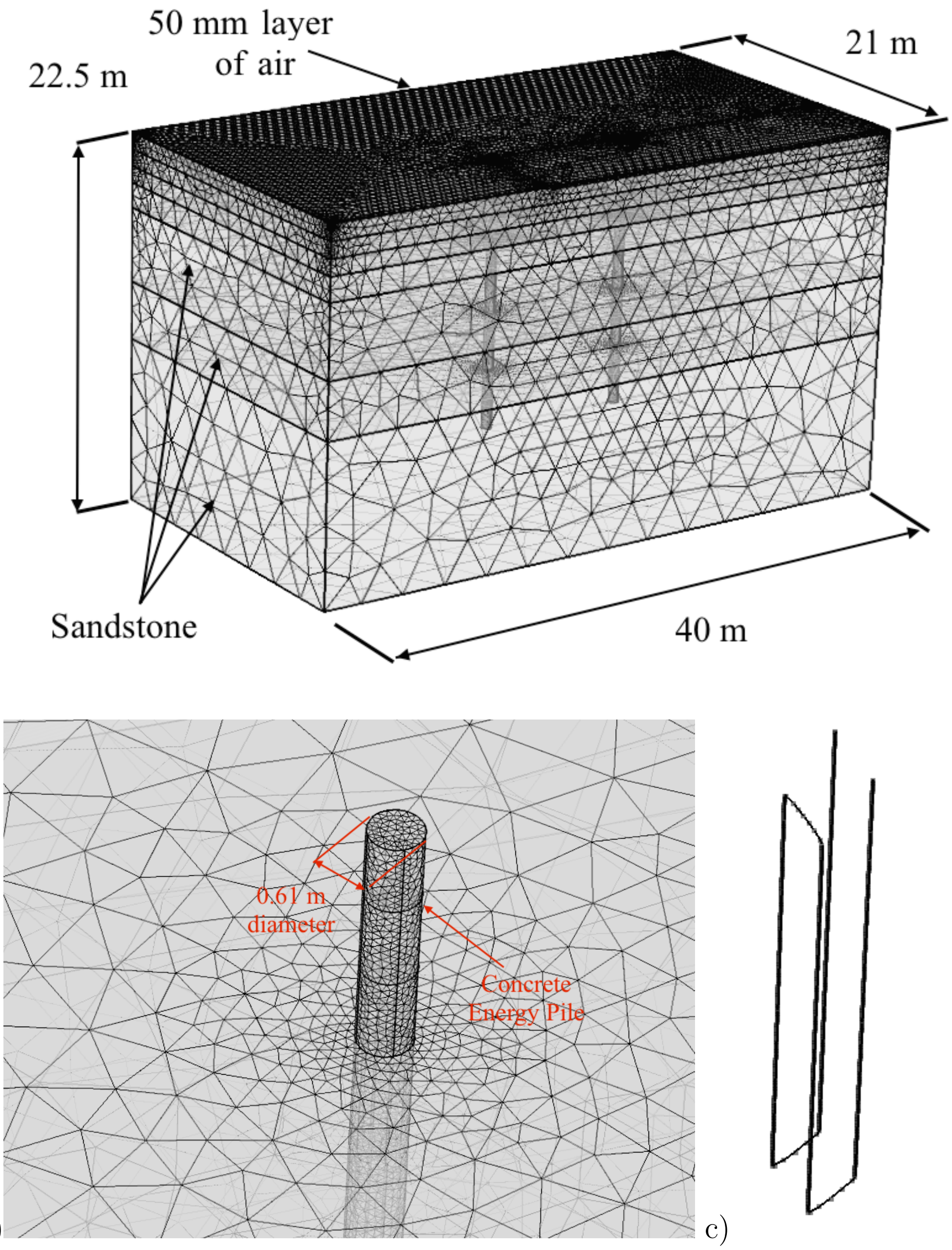

a) b) c)

Figure 7: Refined COMSOL model mesh a) full view b) close up showing pile and element growth c) 1D heat exchanger elements

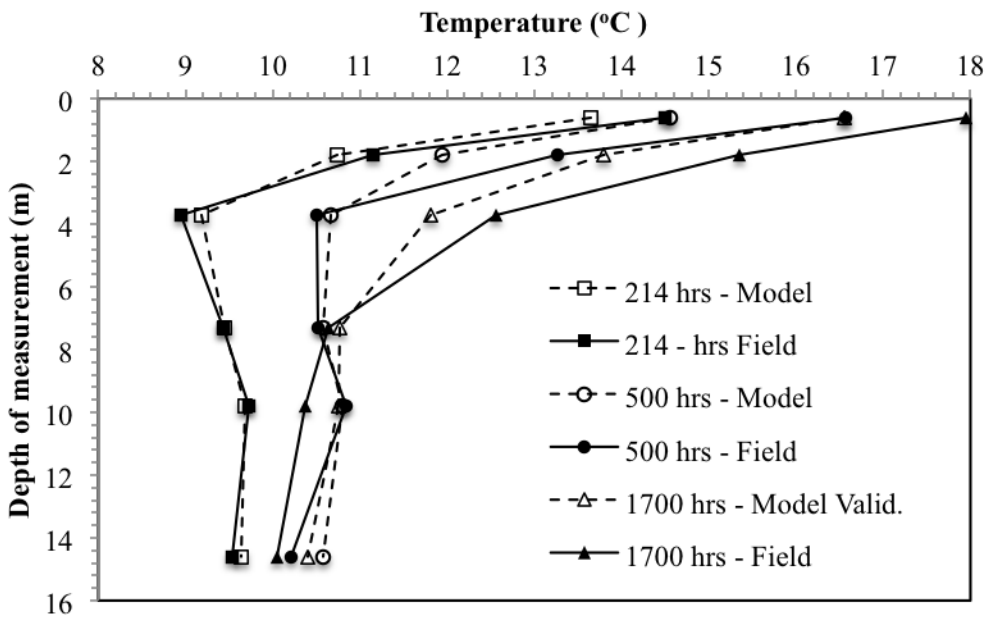

a)

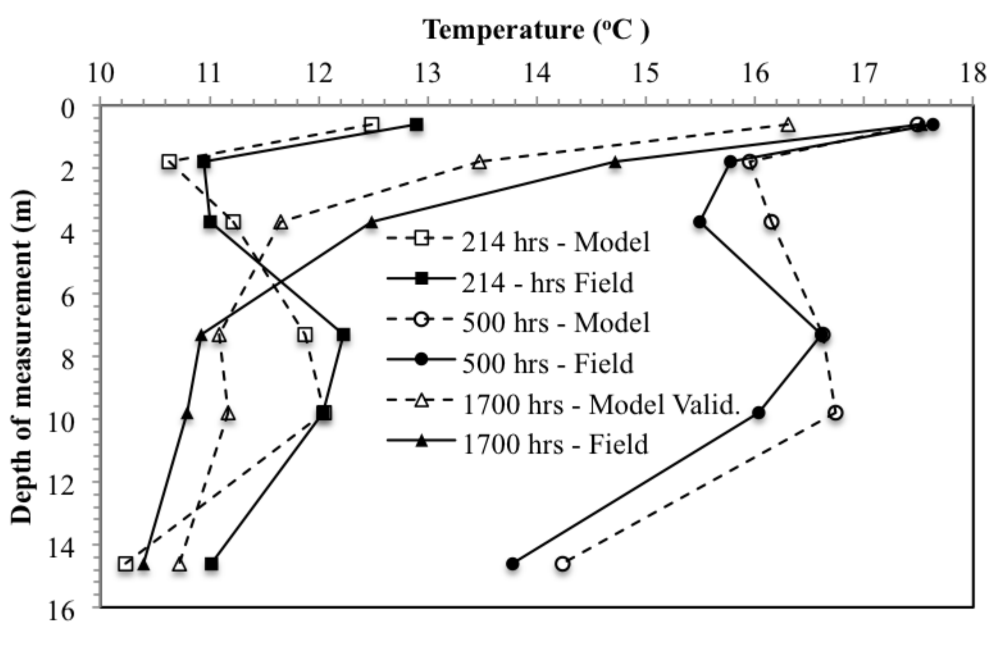

b)

Figure 8: Calibrated model comparison for a) Borehole 6 and b) Borehole 4

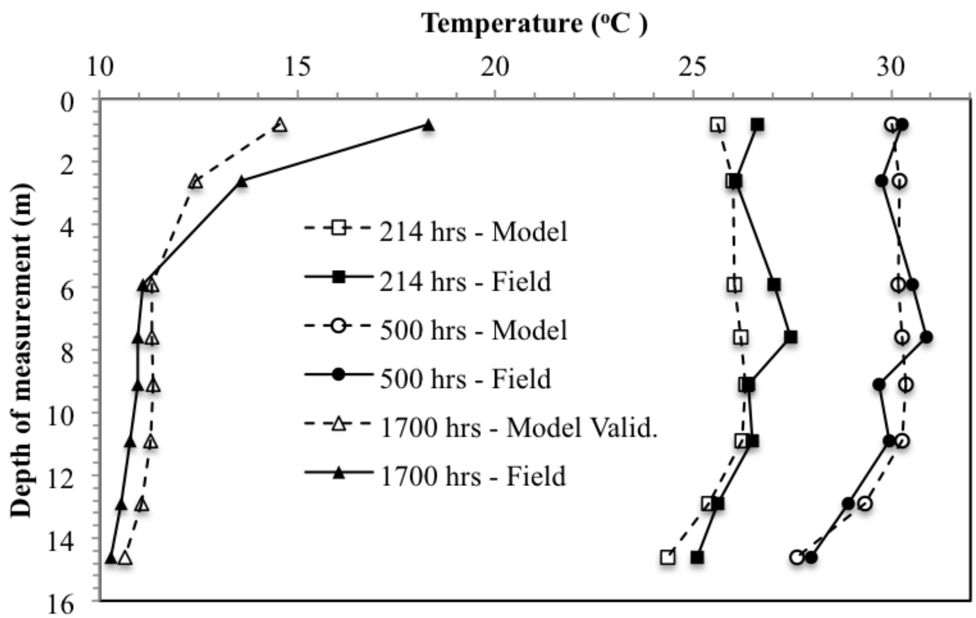

Figure 9: Calibrated model temperature comparison (at strain gauge location) for length of Foundation 4 during heating (214 hours) at the end of heating (500 hours) and at the end of cooling observation (1700 hours)

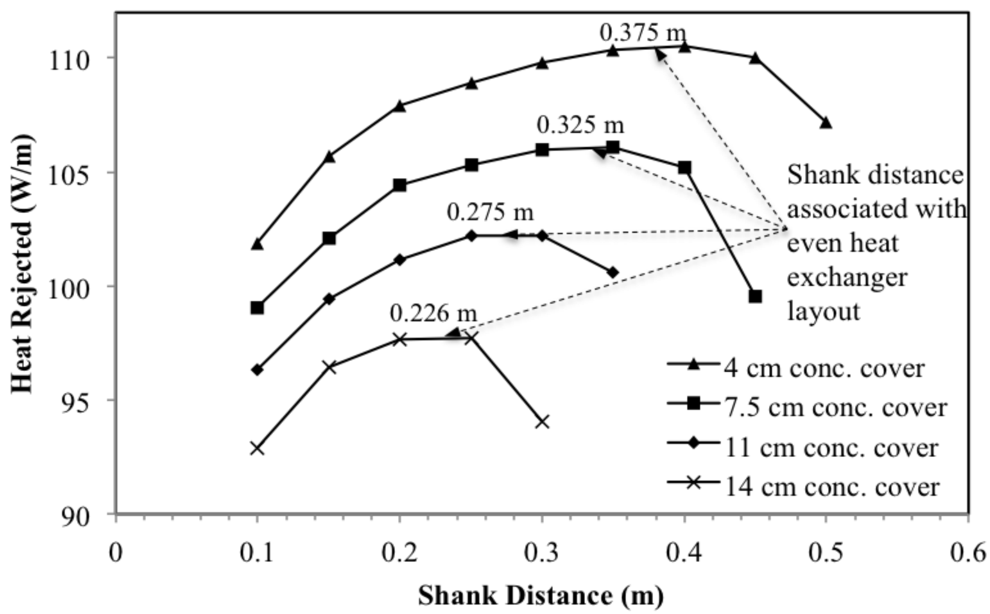

Figure 10: Energy pile heat transfer as a function of shank distance and concrete cover

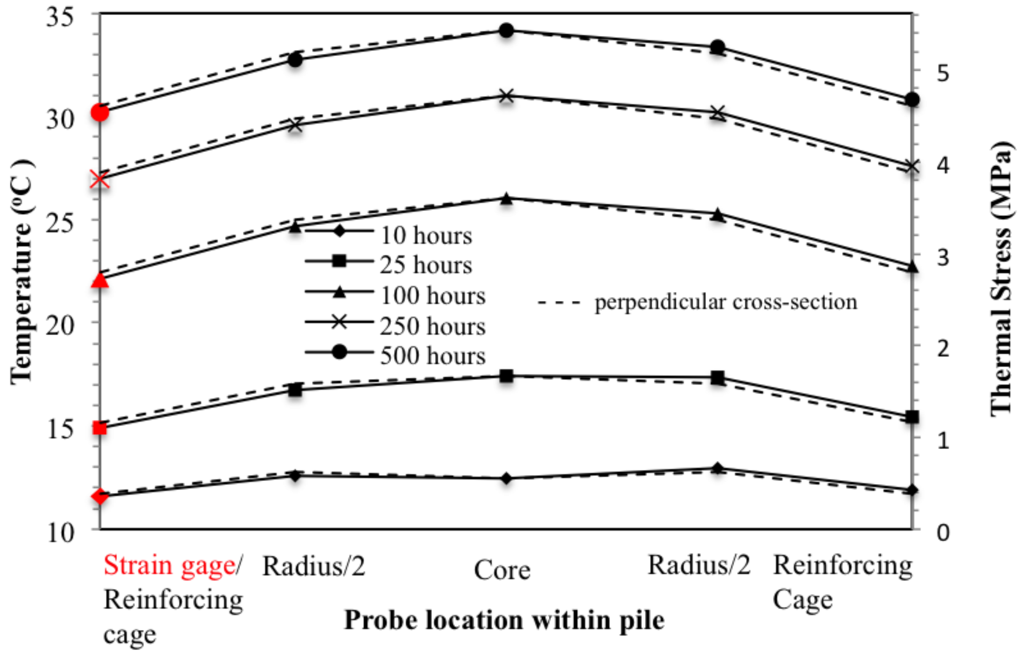

Figure 11: Temperature and thermal axial stress distribution for pile cross section at 7.6 m depth and even heat exchanger distribution

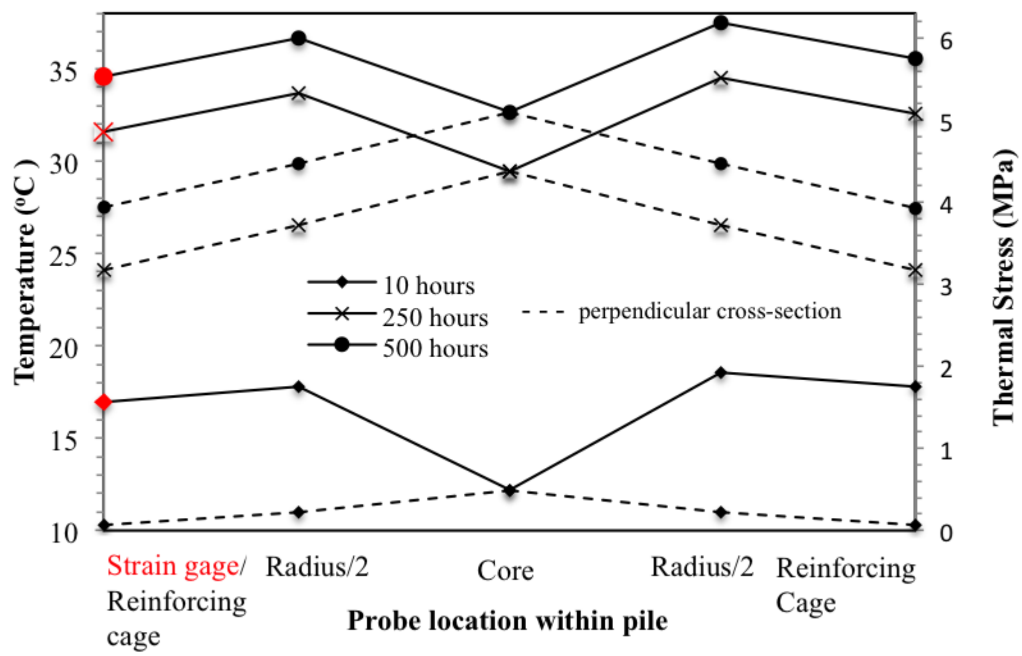

a)

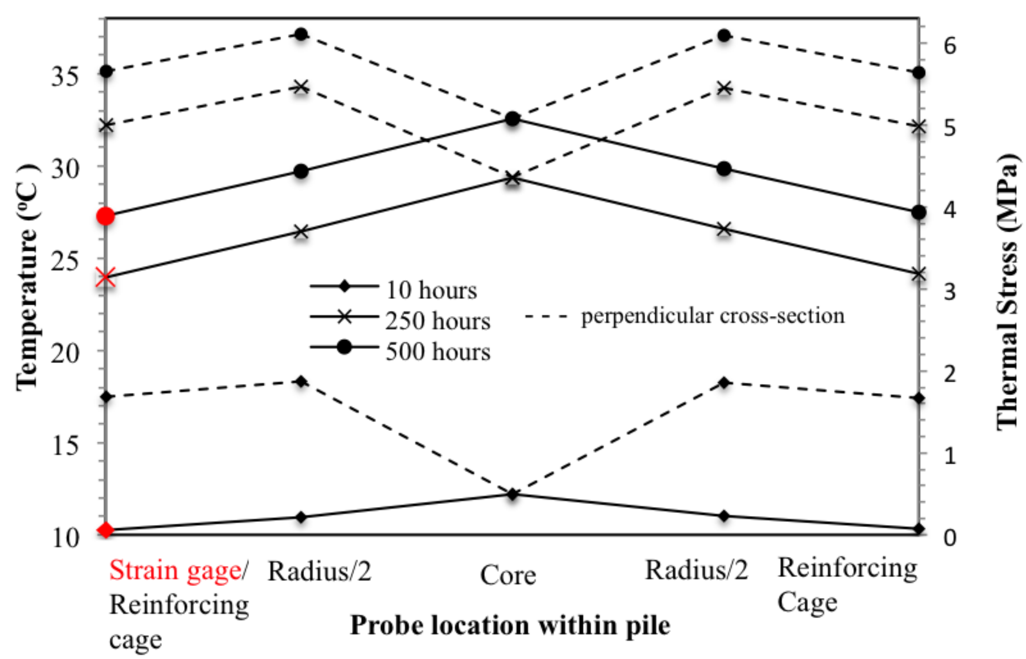

b)

Figure 12: Temperature and thermal axial stress distribution for pile cross section at 7.6 m depth and uneven heat exchanger layouts - shank distances of a) 0.10 m and b) 0.45 m (uneven heat exchanger distributions)

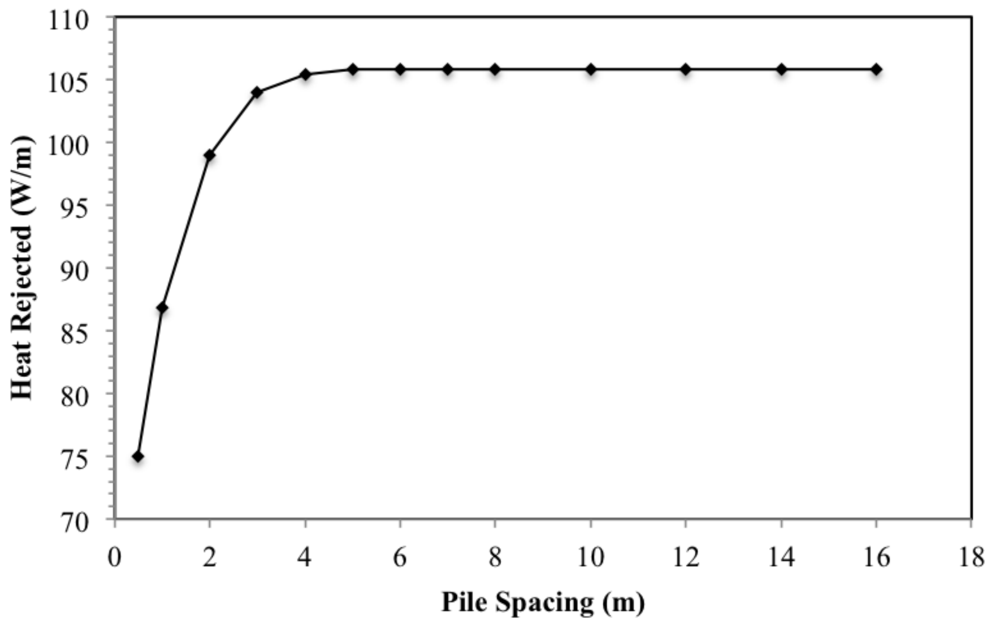

Figure 13: Pile performance as a function of pile spacing

List of Tables

Table 1: Calibrated material properties of COMSOL model

	Property			
Material	Thermal Conductivity $[W/(m*K)]$	Specific Heat Capacity $[J/(kg*K)]$	Density $[kg/m^3]$	Porosity
Sandy Fill (0-1 m)	1.1	860	1875	0.2
Dense Sand (1-2 m)	0.75	935	1957	0.15
Sandstone (2-12.5 m)	1.7	900	2200	0.1
Dense Sandstone (12.5-22.5 m)	1.8	910	2300	0.05
Concrete	1.4	960	2400	-
Glycol/water	0.58	3267	1.008	-
Air	0.023	1010	1.2	-
HDPE (19mm ⌀ 3mm thk)	0.48	-	-	-

Table 2: Foundation 4 model error with respect to field measurements for calibration and validation (three time periods and eight depths)

%Error Foundation 4		Depth (m) 0.8	2.6	5.9	7.6	9.1	10.9	12.9	14.6	Average
Time	214 (calib.)	3.8	0.33	3.75	4.57	0.30	0.95	0.87	3.04	2.20
(hours)	500 (calib.)	0.85	1.52	1.19	1.98	2.28	1.12	1.43	1.20	1.45
	1,700 (valid.)	20.62	8.58	1.89	3.02	3.58	4.81	4.65	3.46	6.32
Average		8.43	3.48	2.28	3.19	2.06	2.30	2.32	2.57	

Table 3: Borehole 4 model error with respect to field measurements for calibration and validation (three time periods and six depths)

%Error		Depth (m)						Average
BH 4		0.6	1.8	3.7	7.3	9.8	14.6	
Time	214 (calib.)	3.15	2.97	1.81	2.83	0.02	7.15	2.99
(hours)	500 (calib.)	0.79	1.12	4.27	0.07	4.36	3.33	2.33
	1,700 (valid.)	6.97	8.48	6.67	1.52	3.52	3.14	5.05
Average		3.64	4.19	4.25	1.47	2.63	4.54	

Table 4: Borehole 6 model output error with respect to field measurements for calibration and validation (three time periods and six depths)

%Error BH 6		Depth (m) 0.6	1.8	3.7	7.3	9.8	14.6	Average
Time	214 (calib.)	5.87	3.69	2.7	0.18	0.52	1.10	2.34
(hours)	500 (calib.)	12.13	9.94	1.51	0.53	0.46	3.59	4.70
	1,700 (valid.)	7.75	10.17	6.02	1.22	3.56	3.50	5.37
Average		8.58	7.94	3.41	0.65	1.52	2.73	